

# The Importance of Singly Charged Oxygen Vacancies for Electrical Conduction in Monoclinic HfO<sub>2</sub>

Michael P. Mueller,<sup>1, a)</sup> Felix Gunkel,<sup>2, b)</sup> Susanne Hoffmann-Eifert,<sup>3</sup> and Roger A. De Souza<sup>1, c)</sup>

<sup>1)</sup>*Institute of Physical Chemistry, RWTH Aachen University, 52056 Aachen, Germany*

<sup>2)</sup>*Peter Gruenberg Institute (PGI 7), Forschungszentrum Juelich GmbH, 52428 Juelich, Germany*

<sup>3)</sup>*Peter Gruenberg Institute (PGI 7 & 10), Forschungszentrum Juelich GmbH, and JARA-FIT, 52428 Juelich, Germany*

(Dated: 13 December 2020)

The point-defect structure of monoclinic HfO<sub>2</sub> (m-HfO<sub>2</sub>) was studied by means of equilibrium electrical conductance measurements as a function of temperature  $1050 \leq T/\text{K} \leq 1200$  and oxygen partial pressure  $-20 \leq \log(p\text{O}_2/\text{bar}) \leq -2$ . The total conductivity  $\sigma$  displayed similar behaviour at each temperature examined. In oxidising conditions ( $p\text{O}_2 \geq 10^{-7}$  bar) the total conductivity increased with increasing oxygen partial pressure, and was assigned to hole conduction. Around  $10^{-10}$  bar a region of almost constant conductivity was found; this is ascribed to ionic conduction by means of doubly charged oxygen vacancies. In reducing conditions ( $p\text{O}_2 \leq 10^{-16}$  bar) the total conductivity, surprisingly, decreased with decreasing oxygen partial pressure. Defect-chemical modelling indicates that this behaviour is consistent with the conversion of mobile doubly charged oxygen vacancies into less mobile singly charged vacancies by electron trapping. Point-defect concentrations at the oxygen partial pressures relevant to resistive switching devices are predicted and discussed.

## I. INTRODUCTION

The electrical conductivity of nominally undoped, monoclinic HfO<sub>2</sub> (m-HfO<sub>2</sub>) has attracted attention for decades, first, out of fundamental interest,<sup>1–4</sup> but recently because of the application of HfO<sub>2</sub> as a gate dielectric or as the active element in Resistive Random Access Memories (ReRAM).<sup>5–14</sup> Despite substantial attention, various aspects of the behaviour are still under debate.

Experimental studies, for example, all report that the conductivity behaviour as a function of oxygen partial pressure ( $p\text{O}_2$ ) differs from that expected for an acceptor-doped oxide (aliovalent impurities in nominally undoped HfO<sub>2</sub> generally being of lower valence than Hf<sup>4+</sup>). The explanations for the observed behaviour also differ, requiring either a coupled transport of oxygen vacancies and interstitials,<sup>1</sup> hafnium vacancies,<sup>2,5</sup> holes<sup>4</sup> or Schottky disorder<sup>3</sup> to play a dominant role. None of these studies take into account the possibility of point defects in other than fully ionised charge states.

The application of HfO<sub>2</sub> in electrical devices initiated computational studies of point defects, and in particular, of defects in various charge states. In the majority of these publications, it is reported that oxygen vacancies in HfO<sub>2</sub> exhibit negative- $U$  properties,<sup>15–20</sup> meaning that singly charged oxygen vacancies are unstable compared

with neutral and doubly charged vacancies:



Such negative- $U$  behaviour is often mistakenly considered to mean that singly charged vacancies will not be present at finite temperature. As long as the energy of reaction (1) is not infinite, however, such defects will be present at all temperatures above absolute zero.<sup>21</sup> The important point here is that the presence of such defects has also been ignored from the computational side.

In order to examine possible changes in the charge states of oxygen vacancies in m-HfO<sub>2</sub>, we measured the total conductivity as a function of oxygen partial pressure in dense m-HfO<sub>2</sub> ceramics at temperatures in the range  $1050 \leq T/\text{K} \leq 1200$  and oxygen partial pressures in the range  $-20 \leq \log(p\text{O}_2/\text{bar}) \leq -2$ . By decreasing the equilibrium oxygen partial pressure, one shifts the Fermi level upwards within the bandgap,<sup>22</sup> thus enabling thermodynamic transition levels to be probed. Numerical defect-chemical calculations were employed to extract quantitative thermodynamic data from  $\sigma(T, p\text{O}_2)$ .

## II. THE STANDARD POINT-DEFECT MODEL OF AN ACCEPTOR-DOPED AO<sub>2</sub> OXIDE

For an acceptor-doped AO<sub>2</sub> oxide, such as CeO<sub>2</sub>,<sup>21,23–25</sup> or YSZ,<sup>26,27</sup> the standard model of the defect chemistry contains four charge carriers (acceptor dopants, electrons, doubly charged oxygen vacancies and holes) and thus involves the electroneutrality condition:

$$[\text{Acc}'] + [e'] = 2[v_{\text{O}}^{\bullet\bullet}] + [h^{\bullet}]. \quad (2)$$

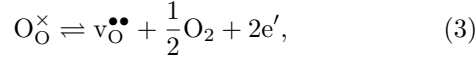
where [def] is the concentration of the defect ‘def’. [Acc'] refers to the effective concentration of all acceptor species

<sup>a)</sup>Author to whom correspondence should be addressed: michael.patrick.mueller@rwth-aachen.de.

<sup>b)</sup>Current address: Department of Energy Conversion and Storage, Technical University of Denmark, DK-2800 Kgs. Lyngby, Denmark

<sup>c)</sup>Electronic mail: desouza@pc.rwth-aachen.de.

and is assumed to be constant. The concentrations of the other three defects vary with  $pO_2$  and  $T$ , and they are linked through two reactions. These are (i) the reduction of the oxide, which takes place according to



with equilibrium constant

$$K_{\text{red}} = \frac{[v_O^{\bullet\bullet}][e']^2 pO_2^{1/2}}{[O_O^\times]} = K_{\text{red}}^\circ \cdot \exp\left(\frac{-\Delta H_{\text{red}}}{k_B T}\right), \quad (4)$$

where  $\Delta H_{\text{red}}$  is the enthalpy of reduction and  $K_{\text{red}}^\circ$  is a pre-exponential factor; and (ii) the generation of electrons and holes by thermal excitation across the bandgap,

$$\text{Null} = h^\bullet + e', \quad (5)$$

with equilibrium constant

$$K_{\text{bg}} = [h^\bullet][e'] = K_{\text{bg}}^\circ \cdot \exp\left(\frac{-E_{\text{bg}}}{k_B T}\right), \quad (6)$$

where  $E_{\text{bg}}$  is the bandgap and  $K_{\text{bg}}^\circ$  is a pre-exponential factor. Solving equations (2), (4) and (6) simultaneously allows the three unknown defect concentrations to be obtained.

The behaviour as a function of  $pO_2$  at constant  $T$  can be divided for typical  $K_{\text{red}}$  and  $K_{\text{bg}}$  into two regimes. In the first regime at lower  $pO_2$ 's, Eq. (2) reduces to  $[e'] = 2[v_O^{\bullet\bullet}]$ . Inserting this condition into Eq. (4) yields

$$[e'] = \left(\frac{2[O_O^\times]K_{\text{red}}}{pO_2^{1/2}}\right)^{1/3} \propto pO_2^{-1/6}. \quad (7)$$

In the second regime at higher  $pO_2$ 's, Eq. (2) changes to  $[\text{Acc}'] = 2[v_O^{\bullet\bullet}]$ , and combination with Eq. (4) yields

$$[e'] = \left(\frac{2[O_O^\times]K_{\text{red}}}{[\text{Acc}']pO_2^{1/2}}\right)^{1/2} \propto pO_2^{-1/4}, \quad (8)$$

and through Eq. (6),

$$[h^\bullet] = \left(\frac{K_{\text{bg}}^2 [\text{Acc}'] pO_2^{1/2}}{2[O_O^\times]K_{\text{red}}}\right)^{1/2} \propto pO_2^{+1/4}. \quad (9)$$

The variations in defect concentrations as a function of  $pO_2$ , as obtained from this standard model, are shown in Fig. 1(a). The complementary behaviour of the conductivities (with electronic mobilities being much higher than ionic mobilities) is shown in Fig. 1(b).

### III. EXPERIMENTAL

Ceramic samples of m-HfO<sub>2</sub> were prepared from commercial powder of HfO<sub>2</sub> (99.95 % purity excluding zirconium, Alfa Aesar®). According to the suppliers' specifications, the main impurities present in the HfO<sub>2</sub> powder are: Zr (2000 ppm), Ca (220 ppm), Si (30 ppm), Al

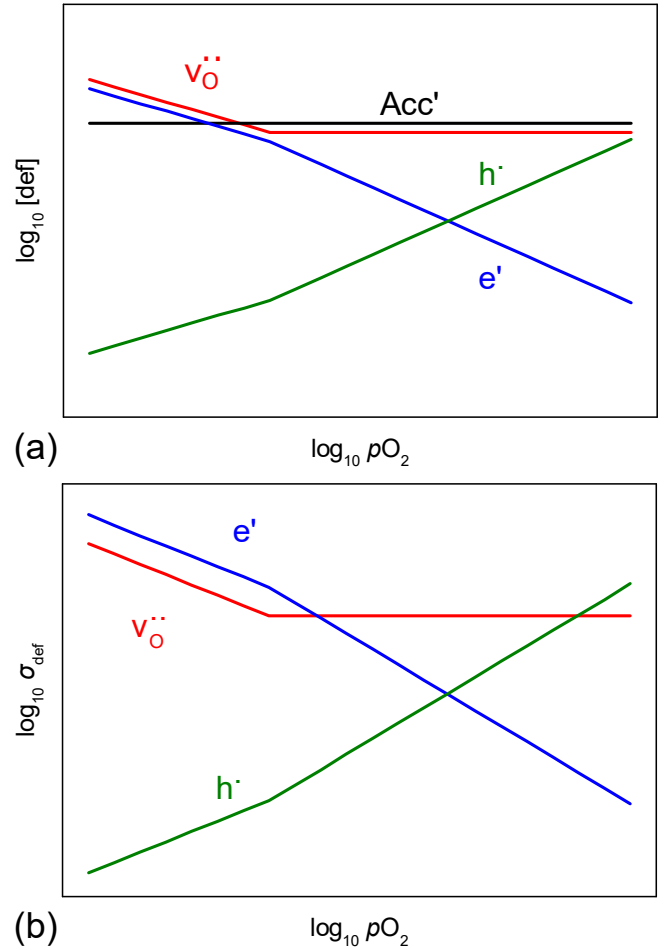


FIG. 1. (Colour online) Schematic diagram of (a) defect concentrations; (b) partial ionic and electronic conductivities in  $AO_2$  as a function of  $pO_2$ .

(25 ppm), Fe (25 ppm) and Ni (18 ppm). This powder was then ball milled with 5 mm ZrO<sub>2</sub> balls and pressed (uniaxially and isostatically) into cylinders with a diameter of 20 mm and a height of 500  $\mu\text{m}$ . The pellets were then sintered at  $T = 1823\text{ K}$  in air for 72 h. The density of the samples was found to be at least 96 % of the theoretical density, measured by Archimedes' principle. X-ray diffractograms (Theta-Theta diffractometer, STOE & Cie GmbH, Darmstadt, Germany) indicated single-phase m-HfO<sub>2</sub>. The grain-size was estimated from scanning electron microscopy images to be  $d_{\text{gr}} \approx 3\text{ }\mu\text{m}$ . High Temperature Equilibrium Conductance (HTEC) was measured in a custom four-point measurement setup utilising an oxygen pump based on yttria stabilised zirconia.<sup>28,29</sup> m-HfO<sub>2</sub> pellets were cut into 5 mm  $\times$  10 mm-wide and 500  $\mu\text{m}$  thin rectangles and connected to the setup by sputtering four platinum contacts on top of the sample. The sputtered contacts were 800  $\mu\text{m}$  wide and ranged over the entire width of the sample. The inner electrodes were spaced 5 mm apart, leading to a square sample geometry of 5 mm  $\times$  5 mm for

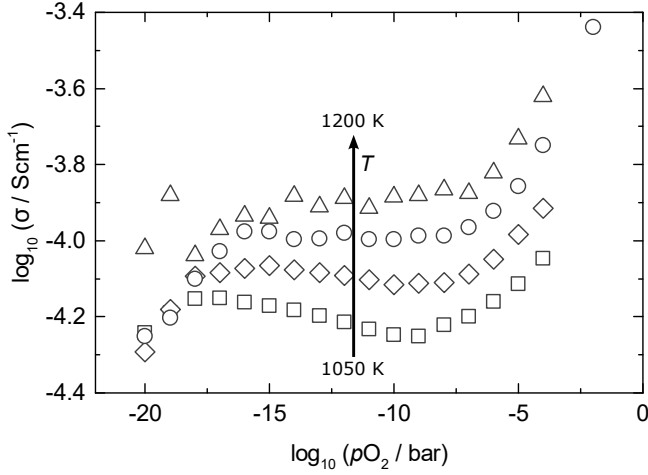


FIG. 2. Conductivity isotherms plotted against oxygen partial pressure for temperature range of  $1050 \leq T/\text{K} \leq 1200$  and oxygen partial pressure range of  $-20 \leq \log(p\text{O}_2/\text{bar}) \leq -2$ .

the measured voltage drop. Then, four thin slits were cut into the sample along the contacts and 100  $\mu\text{m}$  thin platinum wire was wrapped around the slits. Platinum paste was applied to the wire and treated at 1243 K to improve contact. HTEC measurements were performed at temperatures in the range of  $1050 \leq T/\text{K} \leq 1200$  in an  $\text{Al}_2\text{O}_3$  tube furnace and in an oxygen partial pressure range of  $-20 \leq \log(p\text{O}_2/\text{bar}) \leq -2$ . Before measuring each point, a waiting time of  $1 \times 10^4$  s was implemented. HTEC measurements give the conductance  $G$  instead of the conductivity  $\sigma$ . However, all the sample parameters required to obtain the conductivity (length, width and thickness) are known.

#### IV. RESULTS

Fig. 2 shows the conductivity obtained as a function of  $p\text{O}_2$  for four temperatures,  $\sigma(T, p\text{O}_2)$ . In the central region, from  $10^{-16}$  bar to  $10^{-7}$  bar, the conductivity is almost constant. For 1050 K and 1100 K a slight increase in conductivity near the lower pressure end of the plateau was found; this increase was not observed at 1150 K and 1200 K, for which the plateau starts immediately after the reducing regime at  $10^{-16}$  bar. It is also more pronounced for 1050 K, where the plateau is barely visible. Measurements were done in order of decreasing pressure and increasing temperature, so that the sample might have been in a non-equilibrium state in the pressure regime between  $10^{-12}$  bar to  $10^{-2}$  bar for the first two temperatures, which would result in an erroneously low conductivity.

For oxidising conditions,  $p\text{O}_2 > 10^{-7}$  bar for 1050 K, the conductivity increased with increasing  $p\text{O}_2$  for all temperatures. The starting points shifts to higher partial pressures for the higher temperatures. A measurement at  $10^{-2}$  bar is only available for 1150 K, as the other samples

could not be measured at this pressure. The behaviour in the oxidising regime resembles the expected behaviour for undoped  $\text{AO}_2$  oxides, where the conductivity increases at higher  $p\text{O}_2$ 's due to an additional contribution from holes.

In reducing conditions,  $p\text{O}_2 < 10^{-16}$  bar,  $\sigma$  is seen to increase with increasing  $p\text{O}_2$ , and disregarding the two deviating points for 1200 K, this behaviour seems to be largely independent of temperature, since the data points converge at the lowest pressures. The two data points in question for 1200 K exhibited connectivity issues and can therefore be neglected. The behaviour in the reducing regime starkly contrasts the previously described expected behaviour for  $\text{AO}_2$  oxides (see Sec. II).

#### V. DISCUSSION

The conductivity exhibited by m-HfO<sub>2</sub> shows minor, quantitative deviations from the expected behaviour at high  $p\text{O}_2$ 's; an expected plateau at intermediate  $p\text{O}_2$ 's; and major qualitative deviations at low  $p\text{O}_2$ 's. The intermediate regime thus seems, by virtue of being expected, to be the point from which to start analysing the data in detail. To this end we attribute  $\sigma$  in the intermediate regime to ionic conduction arising from doubly positively charged oxygen vacancies. Support for this interpretation comes from molecular dynamics simulations of oxygen-vacancy diffusion.<sup>30</sup> If we take the values of the vacancy diffusivity  $D_v$  obtained in that study, and we convert them into a conductivity with the Nernst-Einstein equation (with  $c_v$  as the oxygen vacancies' concentration and  $z_v e$  as their charge)

$$\sigma = \mu c_v z_v e = \frac{D_v (z_v e)^2 c_v}{k_B T}, \quad (10)$$

we find good agreement for a vacancy concentration of  $2.65 \times 10^{18} \text{ cm}^{-3}$ . This is comparable with values from tracer diffusion studies on the same ceramics.<sup>31</sup>

Now let us turn to the decrease observed at the lowest oxygen partial pressures. Our proposal is that the doubly charged oxygen vacancies trap electrons to form singly charged vacancies:



The equilibrium constant of this reaction is

$$K_{\text{tr},2/1} = \frac{[v_{\text{O}}^{\bullet}]}{[v_{\text{O}}^{\bullet\bullet}][e']} = K_{\text{tr},2/1}^{\circ} \cdot \exp\left(\frac{-\Delta H_{\text{tr},2/1}}{k_B T}\right), \quad (12)$$

with  $\Delta H_{\text{tr},2/1}$  being the corresponding reaction enthalpy. This proposal not only explains why there is no increase in conductivity due to electrons (being trapped, the electrons are not available); but it also explains why the conductivity decreases, provided the singly charged vacancies are not as mobile as the doubly charged vacancies (mobile species are being replaced by less mobile species).

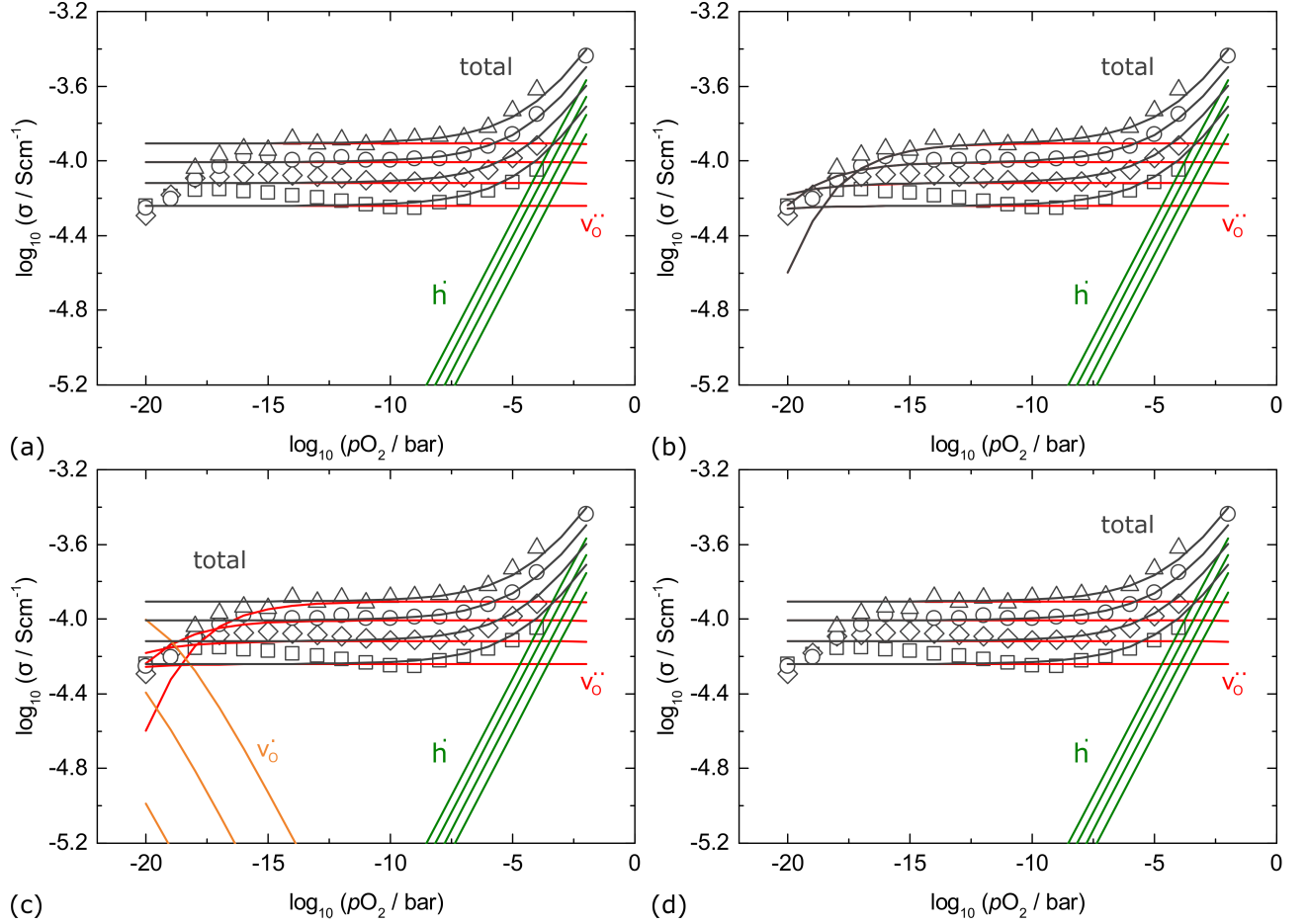


FIG. 3. (Colour online) Conductivity contributions plotted against oxygen partial pressure obtained from defect-chemical calculations for temperature range of  $1050 \leq T/K \leq 1200$  and  $pO_2$  range of  $-20 \leq \log(pO_2/\text{bar}) \leq -2$ . The different graphs are obtained from different calculations. Red lines refer to the conductivity associated with the  $v_O^{\bullet\bullet}$  species; green lines to  $h^\bullet$ ; orange lines to  $v_O^\bullet$  and grey lines to the total conductivity. All calculations contain the electronic excitation equation and the reduction equation; (a) no additional equation; (b) trapping of electrons by  $v_O^{\bullet\bullet}$  to form the significantly less mobile  $v_O^\times$ ; (c) the same as (b) but  $v_O^\bullet$  is as mobile as  $v_O^{\bullet\bullet}$ ; (d) formation of  $v_O^\times$  by electron trapping of  $v_O^{\bullet\bullet}$ .

The second possibility, of doubly charged oxygen vacancies trapping two electrons to form neutral oxygen vacancies,



with equilibrium constant

$$K_{\text{tr},2/0} = \frac{[v_O^\times]}{[v_O^{\bullet\bullet}][e']^2} = K_{\text{tr},2/0}^o \cdot \exp\left(\frac{-\Delta H_{\text{tr},2/0}}{k_B T}\right), \quad (14)$$

can be discounted because the acceptor dopants would be uncompensated. That is, the left-hand-side of Eq. (2) would have  $[Acc']$ , but the right-hand side would have no species, the hole concentration being negligible under reducing conditions and neither singly nor doubly charge oxygen vacancies being present.

Now let us consider the high  $pO_2$  regime. An increase in conductivity along increasing  $pO_2$  is seen, resembling the behaviour expected from an increase in hole concen-

tration. Thus we attribute the conductivity in the high  $pO_2$  regime to holes.

While the proposed explanations are consistent with the observed behaviour, quantitative comparisons provide additional support and allow deeper insights. To that end, numerical defect-chemical modelling was employed to calculate defect concentrations in m-HfO<sub>2</sub> (taking  $[Acc'] = 2[v_O^{\bullet\bullet}] = 5.3 \times 10^{18} \text{ cm}^{-3}$ , see above). The defect mobilities required to calculate individual conductivities, from these defect concentrations, were taken from the literature: for electronic species, we took and modified the electron and hole mobilities determined by Sasaki and Maier<sup>26</sup> for yttria-stabilised ZrO<sub>2</sub>; for oxygen vacancies, we took, as noted above, the values obtained by Schie *et al.*<sup>30</sup>.

Four different models were considered, and the results are compared with the experimental data in Fig. 3. Values for  $K_{\text{red}}$ ,  $K_{\text{bg}}$ ,  $K_{\text{tr},2/1}$  and  $K_{\text{tr},2/0}$ , if required for a specific model, were kept constant for all models. The

first model [Fig. 3(a)] is the standard defect chemical model as presented in Sec. II. Although this model provides an adequate description at high and intermediate  $p\text{O}_2$ 's, it fails at low  $p\text{O}_2$ 's. The second model [Fig. 3(b)] includes the trapping reaction that generates singly charged oxygen vacancies [Eq. (12)] and assumes that these singly charged vacancies have negligible mobility, *i.e.* there is no contribution from the singly charged vacancies to the total conductivity. Of the four models, this model provides the best description of the data.

The last two models confirm particular aspects of our proposed explanation. The question of the mobility of singly charged oxygen vacancies is examined in the third model, in which the trapping reaction [Eq. (12)] is included as before, but now the singly charged vacancies are assumed, for the sake of illustration, to have the same mobility as the doubly charged vacancies. As shown in Fig. 3(c), this model is a worse description of the data at low  $p\text{O}_2$ 's. In this way, the model clearly indicates that  $v_{\text{O}}^{\bullet}$  are less mobile than  $v_{\text{O}}^{\bullet\bullet}$ , confirming the predictions of Duncan *et al.*<sup>20</sup>. It also discounts the alternative possibility, raised by Nakayama *et al.*<sup>32</sup>, of singly charged vacancies being more mobile than the doubly charged vacancies. Finally, the fourth model [Fig. 3(d)] has doubly charged vacancies trapping two electrons to form neutral vacancies [Eq. (14)], as the only trapping reaction. Neutral vacancies of course do not contribute to the conductivity, so the question of their mobility is irrelevant. This model also fails to describe the data at low  $p\text{O}_2$ ; it is essentially indistinguishable from the first model for the reasons given above:  $v_{\text{O}}^{\times}$  do not enter the electroneutrality condition, so their inclusion according to Eq. (14) does not change the concentrations of the charged defect species.

Having obtained a satisfactory description of the conductivity, we discuss briefly the numerical values of the reaction enthalpies used in the description. The bandgap energy of  $E_{\text{bg}} = 5.7\text{ eV}$  is consistent with experimental values reported for m-HfO<sub>2</sub>.<sup>19,33</sup> The reduction enthalpy of  $\Delta H_{\text{red}} = 10.4\text{ eV}$  seems, at first sight, rather high, but it does agree well with computational values: If one combines the energy for the formation of a neutral oxygen vacancy of  $\Delta H_{\text{f}}(v_{\text{O}}^{\times}) = 6.38\text{ eV}$  reported by Scopel *et al.*<sup>34</sup> with energies calculated by Broqvist and Pasquarello<sup>35</sup> for the ionisation from neutral to singly charged vacancies (1.75 eV) and then from singly to doubly charged vacancies (2.05 eV), one obtains a reduction enthalpy of  $\approx 10.2\text{ eV}$ , which is satisfyingly close to the value we used. Lastly, the enthalpy of the trapping reaction that we obtained,  $\Delta H_{\text{tr},2/1} = -2.35\text{ eV}$ , is close to the value obtained by Broqvist and Pasquarello<sup>35</sup> of  $-2.05\text{ eV}$  (the trapping reaction being the inverse of the ionisation reaction).

Although the conductivity data do not probe the transition level for  $v_{\text{O}}^{\bullet}/v_{\text{O}}^{\times}$ , we can calculate a value from our reduction enthalpy and trapping enthalpy if we assume  $\Delta H_{\text{f}}(v_{\text{O}}^{\times})$  from Scopel *et al.*<sup>34</sup>:  $\Delta H_{\text{tr},1/0} = \Delta H_{\text{f}}(v_{\text{O}}^{\times}) - \Delta H_{\text{red}} - \Delta H_{\text{tr},2/1} = -1.67\text{ eV}$ .

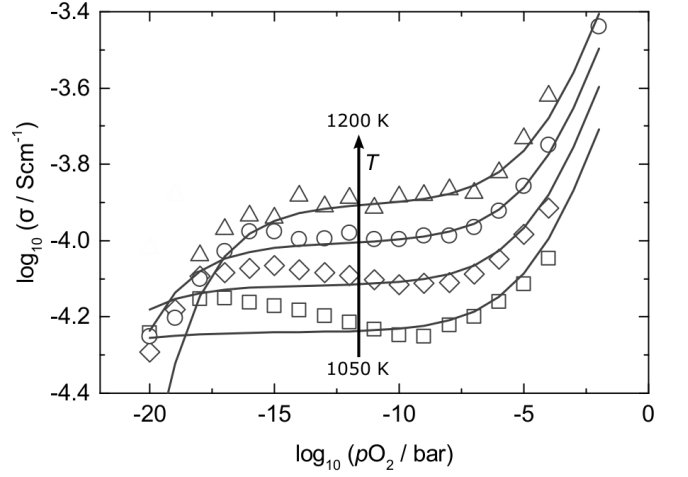


FIG. 4. Conductivity isotherms plotted against oxygen partial pressure for temperature range of  $1050 \leq T/\text{K} \leq 1200$  and oxygen partial pressure range of  $-20 \leq \log(p\text{O}_2/\text{bar}) \leq -2$ . Squares are the measured values, lines are obtained from defect-chemical calculations.

This value should be regarded with caution, as it is not directly obtained. Nevertheless, it indicates that oxygen vacancies are not negative- $U$  species in m-HfO<sub>2</sub>, confirming the predictions of Broqvist and Pasquarello<sup>35</sup>, since the enthalpy of reaction (1) is positive,  $\Delta H = \Delta H_{\text{tr},1/0} - \Delta H_{\text{tr},2/1} = 0.7\text{ eV}$ . For the fourth model, the sum of the two transition levels determined by us was used for Eq. (14). It is  $\Delta H_{\text{tr},2/0} = -4.02\text{ eV}$ .

The mobility of holes, originally taken from Sasaki and Maier<sup>26</sup> (see Table. II), had to be increased by a factor of *ca.* 100 in order to correctly describe the conductivity in the high  $p\text{O}_2$  regime. This is reasonable, since Sasaki and Maier<sup>26</sup> investigated heavily-doped YSZ instead of m-HfO<sub>2</sub>.

Fig. 4 shows the calculated total conductivities from Fig. 3(b) compared to the experimental results. The model presented here is able to reproduce the conductivity over the entire range of  $p\text{O}_2$  quite well. Table I displays the defect reaction energies and pre-exponential parameters and Table II displays the mobilities used for the defect-chemical calculations.

#### A. Oxygen Vacancies at Pressures Relevant to Resistive Switching

In the metal-HfO<sub>2</sub>-metal structures of ReRAMs, the use of a reactive metal as one of the electrodes results in the oxide being strongly reduced, making the understanding of the conductive behaviour in reducing conditions all the more important. If the oxide is in equilibrium with its parent metal, one can calculate the equilibrium partial pressure of oxygen from thermodynamics. The formation of HfO<sub>2</sub> from its elements,



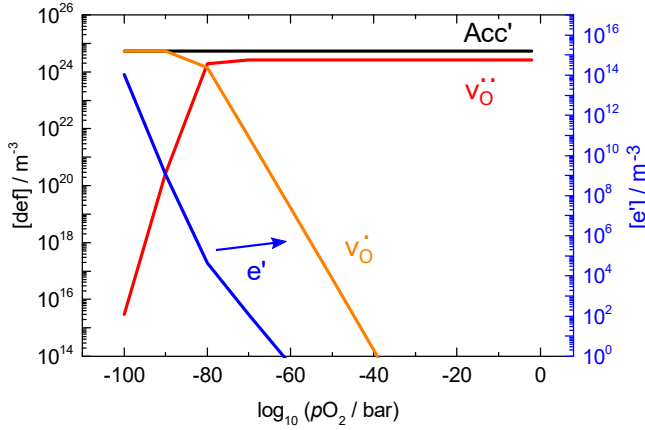


TABLE I. Thermodynamic parameters for m-HfO<sub>2</sub>, with  $k_B = 8.617 \times 10^{-5}$  eV/K.

Reaction	Expression
Reduction	$K_{\text{red}} = 4.18 \times 10^{67} \cdot \exp(-10.4 \text{ eV}/k_B T)$
Electron trapping	$K_{\text{tr},2/1} = 3.46 \times 10^{-29} \cdot \exp(-2.35 \text{ eV}/k_B T)$
Electronic excitation	$K_{\text{bg}} = 1.67 \times 10^{61} \cdot \exp(-5.7 \text{ eV}/k_B T)$

TABLE II. Kinetic parameters for m-HfO<sub>2</sub>, with  $k_B = 8.617 \times 10^{-5}$  eV/K.

Charge carrier	Expression
Oxygen vacancy	$\mu_{v_{\text{O}}^{\bullet\bullet}} = 100/T \cdot \exp(-0.656 \text{ eV}/k_B T)$
Electron	$\mu_e = 6300/T \cdot \exp(-0.55 \text{ eV}/k_B T)^{26}$
Hole	$\mu_h = 100/T \cdot \exp(-0.08 \text{ eV}/k_B T)^{26}$

FIG. 5. (Colour online) Predicted defect concentrations plotted against oxygen partial pressure for a temperature of 500 K and an oxygen partial pressure range of  $-100 \leq \log(p\text{O}_2/\text{bar}) \leq -2$ . NB: the electron concentration is plotted on the right y-axis.

is characterised by a Gibbs energy of formation,  $\Delta G_f(\text{HfO}_2)$ . Writing an equilibrium constant for reaction (15) and setting the activities of the pure condensed phases (Hf and HfO<sub>2</sub>) to unity, one finds

$$p\text{O}_2 = p^\circ\text{O}_2 \cdot \exp\left(\frac{\Delta G_f(\text{HfO}_2)}{k_B T}\right), \quad (16)$$

where  $p^\circ\text{O}_2$  is the standard pressure of 1 bar. At the temperatures relevant for resistive switching (400 K to 600 K),<sup>36</sup> this partial pressure is  $\approx 10^{-100}$  bar.<sup>37</sup> If the Hf|HfO<sub>2</sub> system is not in equilibrium, the effective oxygen partial pressure at the interface will be higher and governed by the time–temperature profile experienced by the system. Switching may then cause selected regions to reach equilibrium.

With the quantitative data obtained from the defect-chemical calculations, it is possible to calculate equilibrium defect concentrations down to the oxygen partial pressures relevant for resistive switching. Fig. 5 shows predicted defect concentrations at  $T = 500$  K for oxygen partial pressures down to  $10^{-100}$  bar. Electrons play a

very insignificant role and their concentration lies more than 10 orders of magnitude below those of the other defects. The amount of singly charged oxygen vacancies present in the system at  $10^{-100}$  bar is  $\sim 5.3 \times 10^{18} \text{ cm}^{-3}$ , meaning that the doubly charged oxygen vacancies are completely replaced and the acceptor dopants are completely compensated by singly charged vacancies. Subsequently, in the very low  $p\text{O}_2$  regime the electroneutrality condition becomes  $[\text{Acc}'] = [v_{\text{O}}^{\bullet}]$  rather than the expected  $[e'] = 2[v_{\text{O}}^{\bullet\bullet}]$ . This indicates that the singly charged oxygen vacancies, which are often neglected in studies investigating the resistive switching properties, are, indeed, important.

## VI. CONCLUSION

From our study of the equilibrium conductivity of monoclinic HfO<sub>2</sub> (m-HfO<sub>2</sub>) as a function of oxygen partial pressure and temperature, we emphasise the following points:

- The results constitute experimental confirmation that oxygen vacancies change their charge state from  $v_{\text{O}}^{\bullet\bullet}$  to  $v_{\text{O}}^{\bullet}$  as the oxide is reduced.
- Quantitative modelling of the defect equilibrium yielded the thermodynamic transition levels for oxygen vacancies changing their charge states and indicated that singly charged oxygen vacancies are less mobile than doubly charged oxygen vacancies.
- The model predicts that singly charged oxygen vacancies play a substantial, if not the dominant, role at the low oxygen partial pressures relevant for resistive switching.

## DATA AVAILABILITY

The data that support the findings of this study are available from the corresponding author upon reasonable request.

## ACKNOWLEDGMENTS

The authors acknowledge funding from the German Research Foundation (DFG) within the collaborative research centre, SFB 917 'Nanoswitches'.

- <sup>1</sup>P. Kofstad and D. J. Ruzicka, On the defect structure of ZrO<sub>2</sub> and HfO<sub>2</sub>, *J. Electrochem. Soc.* **110**, 181 (1963).
- <sup>2</sup>N. M. Tallan, W. C. Tripp, and R. W. Vest, Electrical properties and defect structure of HfO<sub>2</sub>, *J. Am. Ceram. Soc.* **50**, 279 (1967).
- <sup>3</sup>A. Guillot and A. M. Anthony, Interpretation de la conductivité électrique de ZrO<sub>2</sub> et de HfO<sub>2</sub> à haute température (1300°C-1600°C), *J. Solid State Chem.* **15**, 89 (1975).
- <sup>4</sup>V. V. Kharton, A. A. Yaremchenko, E. N. Naumovich, and F. M. B. Marques, Research on the electrochemistry of oxygen ion conductors in the former soviet union, *J. Solid State Electrochem.* **4**, 243 (2000).
- <sup>5</sup>C. Ko, M. Shandalov, P. C. McIntyre, and S. Ramanathan, High temperature electrical conduction in nanoscale hafnia films under varying oxygen partial pressure, *Appl. Phys. Lett.* **97**, 082102 (2010).
- <sup>6</sup>V. Milo, C. Zambelli, P. Olivo, E. Pérez, M. K. Mahadevaiah, O. G. Ossorio, C. Wenger, and D. Ielmini, Multilevel HfO<sub>2</sub>-based RRAM devices for low-power neuromorphic networks, *APL Mater.* **7**, 081120 (2019).
- <sup>7</sup>F. Cüppers, S. Menzel, C. Bengel, A. Hardtdegen, M. von Witzleben, U. Böttger, R. Waser, and S. Hoffmann-Eifert, Exploiting the switching dynamics of HfO<sub>2</sub>-based ReRAM devices for reliable analog memristive behavior, *APL Mater.* **7**, 091105 (2019).
- <sup>8</sup>G. H. Kim, H. Ju, M. K. Yang, D. K. Lee, J. W. Choi, J. H. Jang, S. G. Lee, I. S. Cha, B. K. Park, J. H. Han, T.-M. Chung, K. M. Kim, C. S. Hwang, and Y. K. Lee, Four-bits-per-cell operation in an HfO<sub>2</sub>-based resistive switching device, *Small* **13**, 1701781 (2017).
- <sup>9</sup>S. Clima, Y. Y. Chen, C. Y. Chen, L. Goux, B. Govoreanu, R. Degraeve, A. Fantini, M. Jurczak, and G. Pourtois, First-principles thermodynamics and defect kinetics guidelines for engineering a tailored RRAM device, *J. Appl. Phys.* **119**, 225107 (2016).
- <sup>10</sup>P. Calka, M. Sowinska, T. Bertaud, D. Walczyk, J. Dabrowski, P. Zaumseil, C. Walczyk, A. Gloskovskii, X. Cartoixa, J. Suñé, and T. Schroeder, Engineering of the chemical reactivity of the Ti/HfO<sub>2</sub> interface for RRAM: experiment and theory, *ACS Appl. Mater. Interfaces* **6**, 5056 (2014).
- <sup>11</sup>M. Lanza, K. Zhang, M. Porti, M. Nafria, Z. Y. Shen, L. F. Liu, J. F. Kang, D. Gilmer, and G. Bersuker, Grain boundaries as preferential sites for resistive switching in the HfO<sub>2</sub> resistive random access memory structures, *Appl. Phys. Lett.* **100**, 123508 (2012).
- <sup>12</sup>B. Govoreanu, G. S. Kar, Y.-Y. Chen, V. Paraschiv, S. Kubicek, A. Fantini, I. P. Radu, L. Goux, S. Clima, R. Degraeve, N. Josart, O. Richard, T. Vandeweyer, K. Seo, P. Hendrickx, G. Pourtois, H. Bender, L. Altimime, D. J. Wouters, J. A. Kittl, and M. Jurczak, 10×10nm<sup>2</sup> Hf/HfO<sub>x</sub> crossbar resistive RAM with excellent performance, reliability and low-energy operation, in *IEEE International Electron Devices Meeting 2011* (IEEE, Piscataway, NJ, 2011) pp. 31.6.1–31.6.4.
- <sup>13</sup>Y. Guo and J. Robertson, Materials selection for oxide-based resistive random access memories, *Appl. Phys. Lett.* **105**, 223516 (2014).
- <sup>14</sup>J. Robertson and R. M. Wallace, High-k materials and metal gates for CMOS applications, *Mater. Sci. Eng. R* **88**, 1 (2015).
- <sup>15</sup>C. Shen, M. F. Li, X. P. Wang, H. Y. Yu, Y. P. Feig, A. T. L. Lim, Y. C. Yeo, D. S. H. Chan, and D. L. Kwong, Negative-U traps in HfO<sub>2</sub> gate dielectrics and frequency dependence of dynamic BTI in MOSFETs, in *IEEE International Electron Devices Meeting 2004* (IEEE, Piscataway, N.J., 2004) pp. 733–736.
- <sup>16</sup>J. L. Gavartin, D. M. Ramo, A. L. Shluger, G. Bersuker, and B. H. Lee, Negative oxygen vacancies in HfO<sub>2</sub> as charge traps in high-k stacks, *Appl. Phys. Lett.* **89**, 082908 (2006).
- <sup>17</sup>Y. P. Feng, A. T. L. Lim, and M. F. Li, Negative-U property of oxygen vacancy in cubic HfO<sub>2</sub>, *Appl. Phys. Lett.* **87**, 062105 (2005).
- <sup>18</sup>A. S. Foster, F. L. Gejo, A. L. Shluger, and R. M. Nieminen, Vacancy and interstitial defects in hafnia, *Phys. Rev. B* **65** (2002).
- <sup>19</sup>K. Xiong, J. Robertson, M. C. Gibson, and S. J. Clark, Defect energy levels in HfO<sub>2</sub> high-dielectric-constant gate oxide, *Appl. Phys. Lett.* **87**, 183505 (2005).
- <sup>20</sup>D. Duncan, B. Magyari-Köpe, and Y. Nishi, Filament-induced anisotropic oxygen vacancy diffusion and charge trapping effects in hafnium oxide RRAM, *IEEE Electron Device Lett.* **37**, 400 (2016).
- <sup>21</sup>T. Zacherle, A. Schrieffer, R. A. De Souza, and M. Martin, Ab initio analysis of the defect structure of ceria, *Phys. Rev. B* **87**, 134104 (2013).
- <sup>22</sup>H. Rickert, *Electrochemistry of Solids: An Introduction*, Inorganic Chemistry Concepts, Vol. 7 (Springer, Berlin and Heidelberg, 1982).
- <sup>23</sup>W. C. Chueh and S. M. Haile, Electrochemical studies of capacitance in cerium oxide thin films and its relationship to anionic and electronic defect densities, *Phys. Chem. Chem. Phys.* **11**, 8144 (2009).
- <sup>24</sup>H. L. Tuller and A. S. Nowick, Defect structure and electrical properties of nonstoichiometric CeO<sub>2</sub> single crystals, *J. Electrochem. Soc.* **126**, 209 (1979).
- <sup>25</sup>R. N. Blumenthal, P. W. Lee, and R. J. Panlener, Studies of the defect structure of nonstoichiometric cerium dioxide, *J. Electrochem. Soc.* **118**, 123 (1971).
- <sup>26</sup>K. Sasaki and J. Maier, Re-analysis of defect equilibria and transport parameters in Y<sub>2</sub>O<sub>3</sub>-stabilized ZrO<sub>2</sub> using EPR and optical relaxation, *Solid State Ionics* **134**, 303 (2000).
- <sup>27</sup>C. H. Lee and G. M. Choi, Electrical conductivity of CeO<sub>2</sub>-doped YSZ, *Solid State Ionics* **135**, 653 (2000).
- <sup>28</sup>C. A. Ohly, *Nanocrystalline alkaline earth titanates and their electrical conductivity characteristics under changing oxygen ambients*, Ph.D. thesis, RWTH Aachen University, Germany (2003).
- <sup>29</sup>F. Gunkel, *The role of defects at functional interfaces between polar and non-polar perovskite oxides*, Ph.D. thesis, RWTH Aachen University, Germany (2013).
- <sup>30</sup>M. Schie, M. P. Mueller, M. Salinga, R. Waser, and R. A. De Souza, Ion migration in crystalline and amorphous HfO<sub>x</sub>, *J. Chem. Phys.* **146**, 094508 (2017).
- <sup>31</sup>M. P. Mueller and R. A. De Souza, SIMS study of oxygen diffusion in monoclinic HfO<sub>2</sub>, *Appl. Phys. Lett.* **112**, 051908 (2018).
- <sup>32</sup>M. Nakayama, H. Ohshima, M. Nogami, and M. Martin, A concerted migration mechanism of mixed oxide ion and electron conduction in reduced ceria studied by first-principles density functional theory, *Phys. Chem. Chem. Phys.* **14**, 6079 (2012).
- <sup>33</sup>H. Takeuchi, D. Ha, and T.-J. King, Observation of bulk HfO<sub>2</sub> defects by spectroscopic ellipsometry, *J. Vac. Sci. Technol. A* **22**, 1337 (2004).
- <sup>34</sup>W. L. Scopel, A. Da Silva, JR, W. Orellana, and A. Fazzio, Comparative study of defect energetics in HfO<sub>2</sub> and SiO<sub>2</sub>, *Appl. Phys. Lett.* **84**, 1492 (2004).
- <sup>35</sup>P. Broqvist and A. Pasquarello, Oxygen vacancy in monoclinic HfO<sub>2</sub>: A consistent interpretation of trap assisted conduction, direct electron injection, and optical absorption experiments, *Appl. Phys. Lett.* **89**, 262904 (2006).
- <sup>36</sup>M. Lanza, A review on resistive switching in high-k dielectrics: A nanoscale point of view using conductive atomic force microscope, *Materials* **7**, 2155 (2014).
- <sup>37</sup>T. B. Reed, *Free energy of formation of binary compounds: an atlas of charts for high-temperature chemical calculations* (MIT Press, Cambridge Mass., 1971).